Origin of Enantioselectivity in Asymmetric Hydrovinylations Catalyzed by Phosphoramidite Nickel Catalysts: An Experimentally Supported Density Functional Study

Markus Hölscher, Giancarlo Franciò, and Walter Leitner*

Institut für Technische und Makromolekulare Chemie, RWTH-Aachen, Worringer Weg 1, 52074 Aachen, Germany

Received August 11, 2004

The mechanism of the nickel-catalyzed asymmetric hydrovinylation of styrene in the presence of chiral phosphoramidite ligands was investigated by means of DFT calculations including anion and solvent effects. The theoretical studies are supported by crystal structure analysis and NMR investigations of the ligand. The results obtained indicate that the performance of the catalytically active system is largely affected by a hemilabile coordination mode of one phenyl ring of the phosphoramidite ligand allowing only for two chemically plausible orientations of styrene coordination in the active nickel hydride catalyst. These two diastereomers are the starting points of two reaction paths for hydride transfer to styrene. One path is clearly preferred over the other, as can be deduced from the significantly lower activation energy (+17.57 versus +26.92 kcal/mol) corresponding to the enantiodiscriminating step of the reaction. The displacement of the hemilabily coordinated part of the ligand by ethylene initiates the subsequent reaction paths for C−C bond formation, yielding the *S*- and the *R*-configurated reaction products, respectively. The activation energies show that C−C bond formation does not proceed enantioselectively. Calculations in the presence of anions showed BF_4^--containing systems to be less active than systems with $BARF^-$ (tetrakis-(3,5-bis(trifluoromethyl)phenyl)borate). The results obtained are in accordance with and help to rationalize experimental data.

Introduction

The transition metal catalyzed asymmetric hydrovinylation of styrene or styrene derivatives has proven to be an efficient and highly enantioselective reaction for the formation of carbon−carbon bonds. The products obtained are interesting building blocks for further functionalization since they contain a chiral center in allylic position. In a prototypical reaction styrene **1** and ethylene react to give 3-phenyl-1-butene **2** (Scheme 1). Subsequent catalytic isomerization of **2** to undesired **3** and formation of oligomers can occur as undesired side reactions, the extent depending on the catalytic system.

The hydrovinylation was first reported by Alderson and co-workers in 1965,[1] and ever since this field has been investigated extensively by many research groups. As one result of these efforts, it now appears that catalysts based on nickel and palladium are significantly more active than ruthenium, cobalt, and other metals and/or lead to isomerization of the primary product to a lesser extent.[2]

Scheme 1. Catalytic Hydrovinylation of Styrene

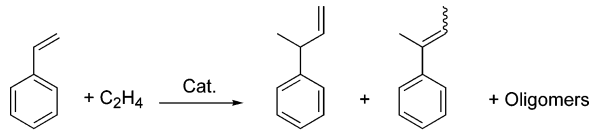

As far as asymmetric hydrovinylation is concerned, the field received pioneering impulses by the work of Bogdanović and Wilke et al.[3a] The Wilke group introduced azaphospholene ligand *all*-(*R*)-**4** and used the corresponding catalyst [{Ni(C_3H_5)(Cl)(*all*-(*R*)-**4**)$_{0.5}$}$_2$] for the enantioselective synthesis of (*R*)-**2**.[3b] This catalyst is extremly active and enantioselective and can be considered as a benchmark system. Recently, we showed that catalysts such as [$Ni_2(C_3H_5)_2(Cl)_2$(*all*-(*R*)-**4**)] can be used in $scCO_2$[4] using NaBARF as chloride-abstracting agent. Moreover a continuous flow system was accomplished using ionic liquids for catalyst immobilization, activation, and tuning, and dense CO_2 as the mobile phase.[5] This has fundamental implications for the potential use in innovative industrial processes.

* Corresponding author. E-mail: leitner@itmc.rwth-aachen.de.

(1) Alderson, T.; Jenner, E. L.; Lindsey R. V. Jr.; *J. Am. Chem. Soc.* **1965**, *87*, 5638.

(2) Jolly, P. W.; Wilke, G. In *Applied Homogeneous Catalysis with Organometallic Compounds*; Cornils, B., Herrmann, W. A., Eds.; VCH: Weinheim, 1996; Vol 2, p 1024.

(3) (a) Bogdanović, B.; Henc, B.; Meister, B.; Pauling, H.; Wilke, G. *Angew. Chem., Int. Ed. Engl.* **1972**, *11*, 1023. (b) Wilke, G. *Angew. Chem.* **1988**, *100*, 189.

(4) Wegener, A.; Leitner, W. *Chem. Commun.* **1999**, 1583.

10.1021/om040107l CCC: $27.50
Publication on Web 10/15/2004

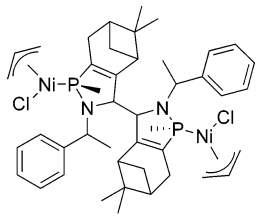

$[Ni_2(C_3H_5)_2(Cl)_2(all\text{-}(R)\text{-}4)]$

Unfortunately the synthesis of the azaphospholene ligand is rather complicated, and all attempts to optimize or simplify the ligand framework substantially have remained unsuccessful. Angermund et al. have investigated the stereoselectivity of Wilke's ligand and related systems on the basis of force field studies comparing the predicted results with experimental data.[6] The authors suggested a "wiper effect" of the phenyl groups attached to the amido part of the ligand and the blocking function of the other half of the dimeric ligand to be influencing the stereoselection process. Furthermore, they considered the geometrical requirements of both the cationic metal complex and the anion. On the basis of these insights they postulated the insertion of styrene into the Ni−H bond to be decisive for enantioselectivity. However, neither was it possible to reduce the amount of synthetic work substantially nor did the modified ligands lead to improved enantioselectivities. To our knowledge this force field study is the only theoretical work reported so far on enantioselective hydrovinylation.

The rational design of other chiral ligands for this reaction has long remained in its infancy. In 1998 RajanBabu et al. used 2-diphenylphosphino-2′-alkoxy-1,1′-binaphthyl (MOP) ligands, which allowed for the hydrovinylation of styrene with enantioselectivities varying between moderate and good.[7] They found that the interplay between coordination ability of the anion and the presence of a hemilabile group in the ligand is crucial for the catalyst stability.[8] In accordance with Wilke and Angermund these authors claimed the styrene coordination to be the stereodiscriminating step.

We recently showed that phosphoramidites, a modularly synthesizable ligand class,[9] perform extremely well also in asymmetric hydrovinylations.[10] Phosphoramidites (R_a,S_c)-**5**, (R_a,R_c)-**6**,[11] and (R_a,S_c,S_c)-**7**[12] yielded enantioselectivities ranging between moderate (56.4% ee), high (87.2% ee), and excellent (94.8% ee), respectively. The Feringa-type ligand also showed a remarkably high activity, reaching TOFs of >1000 at −70 °C.

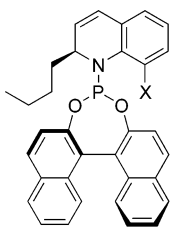

(R_a,S_C)-**5** (X=OMe)

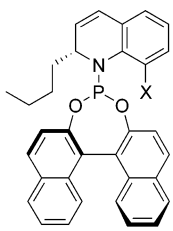

(R_a,R_C)-**6** (X=Cl)

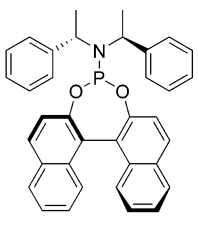

(R_a,S_C,S_C)-**7**

No less important is the fact that ligands **5**, **6**, and **7** are readily available from the synthetic standpoint. The versatility of ligand **7**, its outstanding performance in nickel-catalyzed hydrovinylations, and the lack of a quantum chemical study on this subject prompted us to investigate the reaction mechanism in order to elucidate the origin of enantioselectivity. The theoretical study is based on and is in accordance with experimental results from X-ray structure analysis and NMR spectroscopy.

Computational Details

Calculations in this work were carried out using the Gaussian 98 and 03[13] as well as Turbomole 5.5[14] suite of programs.

Systems without Anions. The structures of complexes using the ligand (R_a,S_c,S_c)-**7** were optimized treating all atoms at the B3LYP/6-31G(d) level of theory as implemented in Gaussian 03 and Gaussian 98. Stationary points were characterized by frequency calculations to prove the existence of local minima (*Nimag* = 0) and transition states of order one (*Nimag* = 1). For transition states IRC calculations were carried out to prove the localized transition states are connecting the localized minima. Table 1 lists energies, zero-point energy corrected energies, and Gibbs free energies for complexes using ligand (R_a,S_C,S_C)-**7** without anions and indicates which compounds were calculated with G98 and G03 (discussion of energies in the text uses the uncorrected energy values *E* throughout this work).

Systems with Anions. Calculations of complexes in the presence of counterions BF_4^- and $BARF^-$ ($BARF^-$ = tetrakis-(3,5-bis-trifluoromethylphenyl)borate) were carried out using the Turbomole 5.5[14] suite of programs taking advantage of the RI-DFT method[15] (there is one exception: $\mathbf{D_{ML}1(BF_4)}$ and $\mathbf{E_{ML}1(BF_4)}$ were calculated using B3LYP/6-31G(d) with Gaussian 98, see text). These calculations were all performed at the

(5) Bösmann, A.; Franciò, G.; Janssen, E.; Solinas, M.; Leitner, W.; Wasserscheid, P. *Angew. Chem. Int. Ed. Engl.* **2001**, *40*, 2697.
(6) Angermund, K.; Eckerle, A.; Lutz, F. *Z. Naturforsch. B* **1995**, *50b*, 488.
(7) Nomura, N.; Jin, J.; Park, H.; RajanBabu, T. V. *J. Am. Chem. Soc.* **1998**, *120*, 459.
(8) (a) RajanBabu, T. V. *Chem. Rev.* **2003**, *103*, 2845. (b) RajanBabu, T. V.; Nomura, N.; Jin, J.; Nandi, M.; Park, H.; Sun, X. *J. Org. Chem.* **2003**, *68*, 8431. (c) RajanBabu, T. V.; Nomura, N.; Jin, J.; Radetich, B.; Park, H.; Nandi, M. *Chem. Eur. J.* **1999**, *5*, 1963. (d) Nandi, M.; Jin, J.; RajanBabu, T. V. *J. Am. Chem. Soc.* **1999**, *121*, 9899.
(9) Catalytic reactions employing **7** as the ligand: Copper-catalyzed asymmetric diethylzinc addition to enones: Feringa, B. L. *Acc. Chem. Res.* **2000**, *33*, 346. Iridium-catalyzed substitution of allylic acetates: Bartels, B.; Helmchen, G. *Chem. Commun.* **1999**, 741. Copper-catalyzed allylic alkylations: Malda, H.; van Zijl, A. W.; Arnold, L. A.; Feringa, B. L. *Org. Lett.* **2001**, *3*, 1169. Rhodium-catalyzed asymmetric olefin hydrogenations: van den Berg, M.; Haak, R. M.; Minnaard, A. J.; de Vries, A. H. M.; de Vries, J. G.; Feringa, B. L. *Adv. Synth. Catal.* **2002**, *344*, 1003. Pena, D.; Minnaard, A. J.; de Vries, J. G.; Feringa, B. L. *J. Am. Chem. Soc.* **2002**, *124*, 14552. van den Berg, M.; Minnaard, A. J.; Haak, R. M.; Leeman, M.; Schudde, E. P.; Meetsma, A.; Feringa, B. L.; de Vries, A. H. M.; Jaljaars, C. E. P.; Williams, C. E.; Hyett, D.; Boogers, J. A. F.; Henderickx, H. J. W.; de Vries, J. G. *Adv. Synth. Catal.* **2003**, *345*, 208. Palladium-catalyzed asymmetric Heck reactions: Imbos, R.; Minnaard, A. J.; Feringa, B. L. *J. Am. Chem. Soc.* **2002**, *124*, 184. Rhodium-catalyzed asymmetric arylation of enones: Imbos, R. Dissertation, University of Groningen, 2002. Palladium-catalyzed asymmetric hydrogenations of olefins: Jensen, J. F.; Svendsen, B. Y.; La Cour, T. V.; Pedersen, H. L.; Johannsen, M. *J. Am. Chem. Soc.* **2002**, *124*, 4558. Iridium catalyzed allylic amination and etherification: Ohmura, T.; Hartwig, J. F.; *J. Am. Chem. Soc.* **2002**, *124*, 15164. Lopez, F.; Ohmura, T.; Hartwig, J. F. *J. Am. Chem. Soc.* **2003**, *125*, 3426.
(10) Franciò, G.; Faraone, F.; Leitner, W. *J. Am. Chem. Soc.* **2002**, *124*, 184.
(11) Franciò, G.; Arena, C. G.; Faraone, F.; Graiff, C.; Lanfranchi, M.; Tiripicchio, A.; *Eur. J. Inorg. Chem.* **1999**, 1219.
(12) Feringa, B. L.; Pineschi, M.; Arnold, L. A.; Imbos, R.; de Vries, A. H. M. Angew. Chem. **1997**, *109*, 2733.
(13) *Gaussian 98*, Revision A. 11; *Gaussian 03*, Revision B.03; Gaussian, Inc.: Pittsburgh, PA, 2003.
(14) *Turbomole 5.5*; Quantum Chemistry Group, University Karlsruhe 1988.
(15) Eichkorn, K.; Treutler, O.; Öhm, H.; Häser, M.; Ahlrichs, R. *Chem. Phys. Lett.* **1995**, *240*, 283.

Table 1. Energies *E*, Zero-Point Energy Corrected Energies E_{Zpe}, Gibbs Free Energies *G* (all in Hartree) and Number of Imaginary Frequencies (*Nimag*) for Complexes B−E Calculated at the B3LYP/B1 Level of Theory[a]

compd	*E*	E_{zpe}	*G*	*Nimag*[b]
A	−3445.0104	−3444.4324	−3444.4984	0
B1	−3754.7619	−3754.0443	−3754.1200	0
B1a	−3754.7307	−3754.0156	−3754.0918	0
B2	−3754.7641	−3754.0465	−3754.1223	0
B3	−3754.7577	−3754.0403	−3754.1169	0
B4	−3754.7577	−3754.0403	−3754.1169	0
B6	−3754.7334	−3754.0193	−3754.0970	0
B8	−3754.7347	−3754.0203	−3754.0971	0
C1	−3754.7697	−3754.0516	−3754.1263	0
C2	−3754.7673	−3754.0491	−3754.1237	0
D1	−3833.3675	−3832.5936	−3832.6717	0
D2	−3833.3658	−3832.5918	−3832.6702	0
D3a	−3833.3709	−3832.5971	−3832.6746	0
E1	−3833.3900	−3832.6137	−3832.6905	0
E2	−3833.3883	−3832.6116	−3832.6876	0
E3	−3833.3838	−3832.6074	−3832.6831	0
TS(B1−C1)	−3754.7339	−3754.0179	−3754.0929	1 (−135.3)
TS(B2−C2)	−3754.7212	−3754.0054	−3754.0814	1 (−142.0)
TS(D1−E1)	−3833.3570	−3832.5829	−3832.6605	1 (−213.8)
TS(D2−E2)	−3833.3563	−3832.5820	−3832.6604	1 (−211.9)
TS(D3−E3)	−3833.3523	−3832.5778	−3832.6540	1 (−206.3)
ethylene (G98)	−78.5870	−78.5362	−78.5584	0
ethylene (G03)	−78.5874	−78.5362	−78.5571	0
styrene (G98)	−309.6483	−309.5145	−309.5460	0
styrene (G03)	−309.6483	−309.5146	−309.5462	0

[a] Compounds **B** and **C** and corresponding transition states were calculated using Gaussian 03; compounds **D** and **E** as well as corresponding transition states were calculated using Gaussian 98. [b] Values in parentheses denote imaginary wavenumbers [cm^{-1}].

Table 2. Energies *E* [Hartree] and Energies Obtained Using the Inclusion of Solvent Effects by the COSMO Method E_{Cosmo} [Hartree] for Complexes C Calculated at the BP86/SV(P) Level of Theory[a]

compd	*E*	E_{COSMO}
BF_4:		
C1	−3753.6091	−3753.6561
C2	−3753.6072	−3753.6541
C1(BF_4)-1	−4177.9229	−4177.9544
C1(BF_4)-2	−4177.9052	−4177.9455
C1(BF_4)-3	−4177.9115	−4177.9499
C1(BF_4)-4	−4177.9494	−4177.9696
	(−4180.7976)	(−4180.8213)
C2(BF_4)-4	−4177.9431	−4177.9649
	(−4180.7939)	(−4180.8197)
BARF:		
C1(barf)-1	−7399.0640	−7399.0942
C1(barf)-2	−7399.0597	−7399.0948
C1(barf)-3	−7399.0590	−7399.0947
C2(barf)-1	−7399.0607	−7399.0911
BF_4^-	−424.2008	−424.2852
$BARF^-$	−3645.3898	−3645.4279

[a] These calculations were carried out using the RI-DFT method.[15] Values in parentheses denote the results of geometry optimizations carried out at the BP86/TZVP level of theory.

BP86 level of theory using the SV(P) basis set as implemented in Turbomole 5.5 for all elements. Solvation effects were included in some of the calculations using the COSMO solvation approach.[16] Energies of anion-containing systems are listed in Table 2 (some compounds were also optimized at the BP86/TZVP level of theory, Table 2).

Note: The studies on the anion-free systems were the starting point for the study presented here. Gaussian98 was available for us solely at that time, and the computational cost was figured to be too large to include anion-containing systems in the study. However during the course of the studies

Scheme 2. Generally Accepted Hydrovinylation Mechanism (X = anion, L = ligand, D = functional group interacting as hemilabile donor)[a]

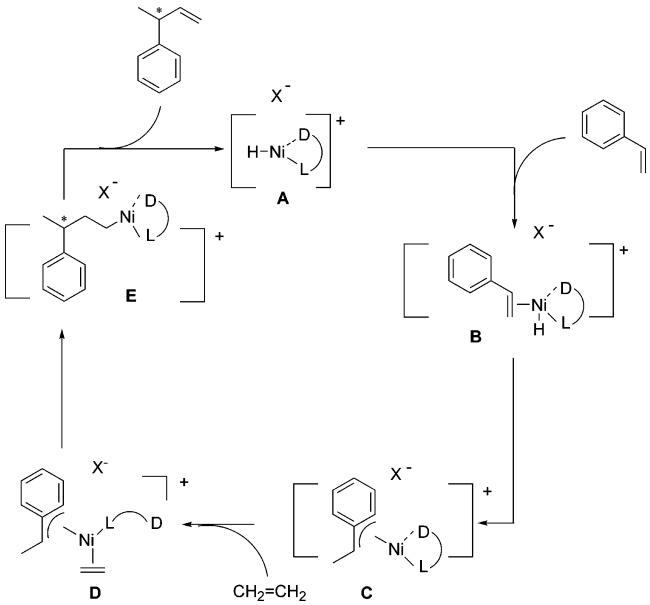

[a] The strength of the interaction between cation and anion as well as cation and hemilabile donor depends on the size and chemical nature of both species (see text).

Turbomole 5.5 became available to us, and the RI-DFT method implemented in Turbomole reduces computation times considerably, which made it possible to treat some anion-containing systems with this method. However, the RI-DFT method works only for pure DFT functionals, which explains why BP86 was chosen here instead of B3LYP. Due to this difference, the energies of anion-free and anion-containing systems cannot be compared. The results reported on the anion-containing systems stand as are. Also Gaussian03 became available later during the study, which shows much better computational efficiency than its predecessor, which prompted us to continue the study with this software. Since we had noted with earlier versions of the Gaussian program series that the energies always differ slightly from version to version, we recalculated some geometries/energies (which is noted in Table 1) to ensure the differences are small enough not to distort the conclusions drawn from the results.

Results and Discussion

Mechanism Hypotheses. It is generally accepted that a nickel hydride mechanism is most likely to apply for this type of reaction, and numerous groups have contributed to its understanding.[17] The coordination of styrene to cationic nickel hydride **A** leads to intermediate **B**, followed by insertion into the Ni−H bond to give the more stable **C**. In **C** the styrene moiety is η^3-bonded in an allyl type coordination. In the next step ethylene coordinates to the complex, generating **D**. Then, the C−C bond forming reaction takes place and yields **E**, which by β-hydride elimination yields the hydrovinylated product and hydride **A** (Scheme 2).

(16) (a) Klamt, A.; Schüürmann, G.; *J. Chem. Soc., Perkin Trans. 2* **1993** 799. (b) Andzelm, J.; Koelmel, C.; Klamt, A. *J. Chem. Phys.* **1995**, *103*, 9312.

(17) (a) Bogdanović, B. *Adv. Organomet. Chem.* **1979**, *17*, 105. (b) Keim, W. *Angew. Chem.* **1990**, *102*, 251. (c) Müller, U.; Keim, W.; Krüger, C.; Betz, P. *Angew. Chem.* **1989**, *101*, 1066. (d) DiRenzo, G. M.; White, P. S.; Brookhart, M.; *J. Am. Chem. Soc.* **1996**, *118*, 6225. (e) DiRenzo, G. M.; Ph.D. Thesis, University of North Carolina, 1997.

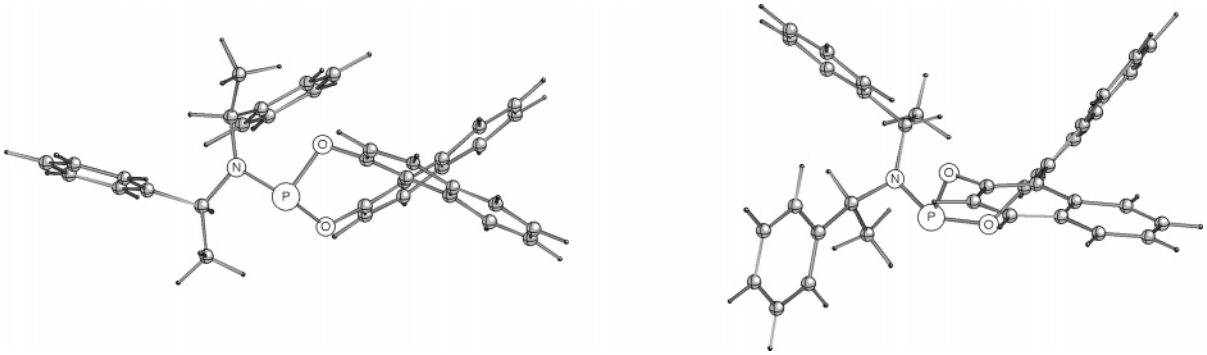

Figure 1. Geometries of (R_a,S_C,S_C)-**7** with the highest (left) and the lowest (right) energy as calculated at the B3LYP/6-31G(d) level of theory.

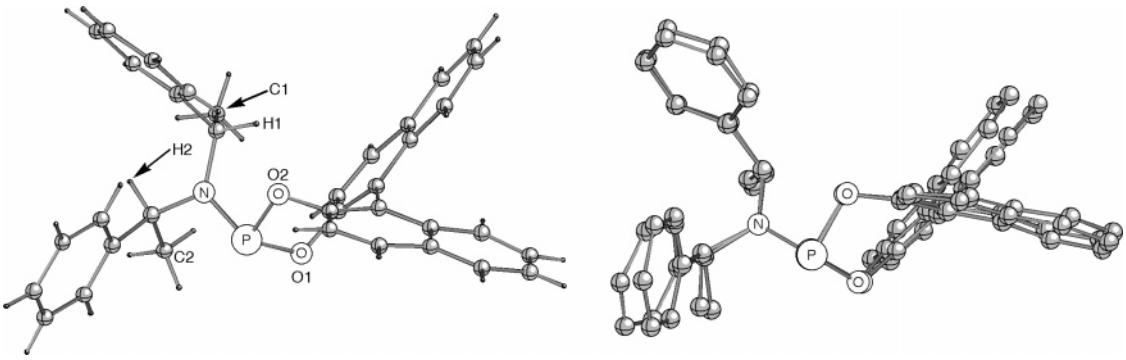

Figure 2. (Left) Structure of (R_a,S_C,S_C)-**7** in the solid state. Selected atom distances [Å] and angles [deg]: P−O1 1.661, P−O2 1.663, P−N 1.658; O2−P−O1 98.04, N−P−O2 109.68, N−P−O1 96.01. (Right) Superimposition of the calculated and the solid state structure of (R_a,S_C,S_C)-**7** (hydrogen atoms were removed for clarity).

Also the mechanism includes the presence of the anion, which interacts attractively with the cationic nickel complexes at certain stages of the cycle. The strength of this interaction can be assumed to vary most likely between strong and weak depending on the size and chemical nature of the anion. Furthermore hemilabile coordination by donor groups of the ligand can play a role when ligands with appropriate functional groups are used.[8] For the present study we use this mechanism as a working hypothesis.

Crystal Structure Analysis and NMR Spectroscopic Studies of the Ligand. Theoretical studies aiming at full geometry optimizations of relevant stationary points of the hypersurface for accurate energies rely on preexisting knowledge of the complex and/or ligand structures. With monodentate ligands of the size and conformational flexibility as (R_a,S_C,S_C)-**7** a theoretical screening combined with experimental data is necessary to obtain a reasonable ligand structure. By supplying plausible starting geometries for optimizations, we located four different conformers of (R_a,S_C,S_C)-**7**, with the highest and lowest energy conformer differing in energy by 6.46 kcal/mol at the B3LYP/6-31G(d) level of theory (Figure 1).

It is evident from Figure 1 that the relative orientation of the substituents within the amido part differs substantially for the individual conformers. It is interesting to note that the thermodynamically most favored conformer does not exhibit C_2 symmetry. This result was confirmed by an X-ray structure analysis on crystals of (R_a,S_C,S_C)-**7**[18,19] prior to computational investigations. The structure obtained is shown in Figure 2.

In the solid state (R_a,S_C,S_C)-**7** adopts a unique geometry far away from C_2-symmetry. The binaphthyl substituent shows no anomalies, and bond lengths and angles are within expected ranges. The nitrogen atom is surrounded nearly ideally trigonal planar with an angle sum at N of 359.7°. This is in accord with the negligible basicity of the nitrogen center of phosphoramidites that coordinate solely via phosphorus. The two methyl groups C1 and C2 of the amido substituents point nearly in the same direction. The hydrogen atom H1 is oriented toward the binaphthyl system, whereas H2 points to the opposite direction. Most interesting is the relative orientation of the two phenyl rings, which are arranged almost perpendicular. The solid state structure of (R_a,S_C,S_C)-**7** and the lowest energy structure calculated at the B3LYP/6-31G(d) level of theory are superimposable with no substantial deviations (Figure 2), indicating that packing forces do not account significantly for this conformation in the solid state.

Also the solution structure of (R_a,S_C,S_C)-**7** was studied extensively by NMR spectroscopy. A systematic NMR study revealed different chemical shifts for both halves of the binaphthyl moiety at room temperature, whereas the spectrum of the amido substituent is simple because of fast rotation around the N−P bond. At −70 °C the

(18) Crystal structure of (R_a,S_C,S_C)-**7**: Crystals suitable for X-ray structure analysis were grown by slow diffusion of pentane into a CH_2Cl_2 solution of (R_a,S_C,S_C)-**7** at −18 °C. Colorless needles, ca. 0.8 × 0.5 × 0.4 mm^3, Enraf-Nonius-CAD-4 diffractometer, Mo Kα, λ = 0.71073 Å, T = −30 °C, M_r = 624.51, monoclinic, a = 9.5945(4) Å, b = 15.8414(10) Å, c = 10.7864(5) Å, β = 106.49(3)°, V = 1572.0(14), Z = 2, space group $P2_1$ (No. 4), ς_{calc} = 1.319 g cm^{-3}, 14 512 measured reflections, 6857 unique reflections, 5713 unique reflections with $I > 4\sigma(I)$, full matrix least squares refinement on F^2, $R[I>4\sigma(I)]$ = 0.0684, R = 0.0828 (all data), wR_2 = 0.20007, GOF = 1.023, Flack parameter = 0.086. The structure contains two CH_2Cl_2 molecules per unit cell.

(19) The structure of an iridium complex containing ligand (S_a,S_C,S_C)-**7** was reported: Kiener, C. A.; Shu, C.; Incarvito, C.; Hartwig, J. F. *J. Am. Chem. Soc.* **2003**, *125*, 14272.

Scheme 3. Hypothetical Diastereomers B Formed by Coordination of Styrene to Nickel Hydride A with the Hydride *trans* to P (a) and *cis* to P (b)[a]

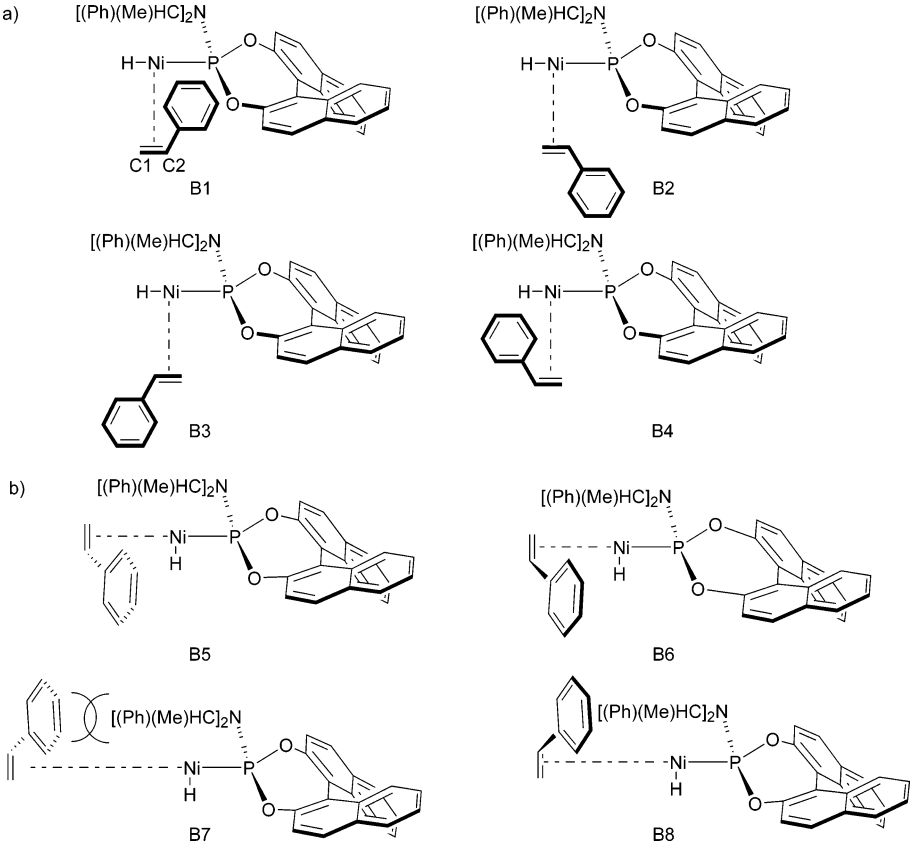

[a] C1 is the terminal and C2 the internal carbon atom of the olefinic double bond (shown for B1). B7 cannot be built. In (a) the atoms P, Ni, C1, C2 and the hydride H bound to Ni reside in one plane, which can be envisioned best with the P−Ni−H vector residing in the drawing plane and the styrene molecule being in front of the drawing plane. The fourth coordination site of the quadratic planar environment of the nickel center is behind the drawing plane and is occupied by parts of the ligand.

NMR spectrum revealed that this rotation around the N−P bond is frozen out. The room-temperature H−H and H−P NOEs were studied as well as the ROESY spectrum at −70 °C (this temperature was also used for the hydrovinylation reactions[10]). These NMR studies reveal that the relative arrangement of the substituents in the amido part of the ligand is very similar to the structure in the solid state; that is, the solid state conformation is largely preserved in solution at low temperatures. Thus, it is plausible to use the solid state structure of the ligand as input for the calculation of the corresponding nickel complexes.

Computational Studies

Coordination of Styrene and Hydride Transfer (B → C). The study was started by investigating monocationic nickel hydride complexes **B** using the crystal structure of (R_a,S_C,S_C)-**7** for generating starting structures. The size and shape of (R_a,S_C,S_C)-**7** suggest an occupation of two of the four coordination sites of a quadratic planar coordinated Ni^{2+} center; one site is occupied by a real coordination of the phosphours center, and one by "blocking" an adjacent coordination site via the shielding effect of one phenyl substituent in the amido part of the ligand. From simply generating reasonable starting structures it could not be decided at this stage if this blocking was a mere occupation of space or an attractive interaction by hemilabile coordination. The third and fourth coordination sites are occupied by hydride and styrene, respectively. These two positions can be exchanged, which yields eight different diastereomers (Scheme 3). One of these (**B7**) can simply not be generated, since the styrene molecule would clash directly with parts of the ligand. The remaining seven diasteromers can be built, and most of them can be relaxed to local minima (vide infra).

From these seven possibilities there are only three diastereomers that are catalytically competent with regard to the hydride transfer step: The hydride must be transferred to the terminal carbon atom (C1, Scheme 3) of the olefinic double bond, which will be the case starting from **B1**, **B2**, and **B8**. A hydride transfer to the internal carbon atom (C2) of the olefinic double bond would finally yield linear products, which are never observed experimentally as primary products of the catalytic cycle (in this work we do not address any isomerization reactions whatsoever).

For completeness we performed full geometry optimizations of all seven diastereomers. The key structural feature of the diastereomers **B** which were located computationally is that one phenyl ring of the ligand is indeed interacting attractively with the nickel center, resulting in a distorted square planar coordination sphere for nickel. Structures **B1**−**B4** and **B6** were located, **B5** could not be located, and for **B8** only a conformation with perpendicular olefin coordination was found. Furthermore for structures **B1**−**B4** the nickel-

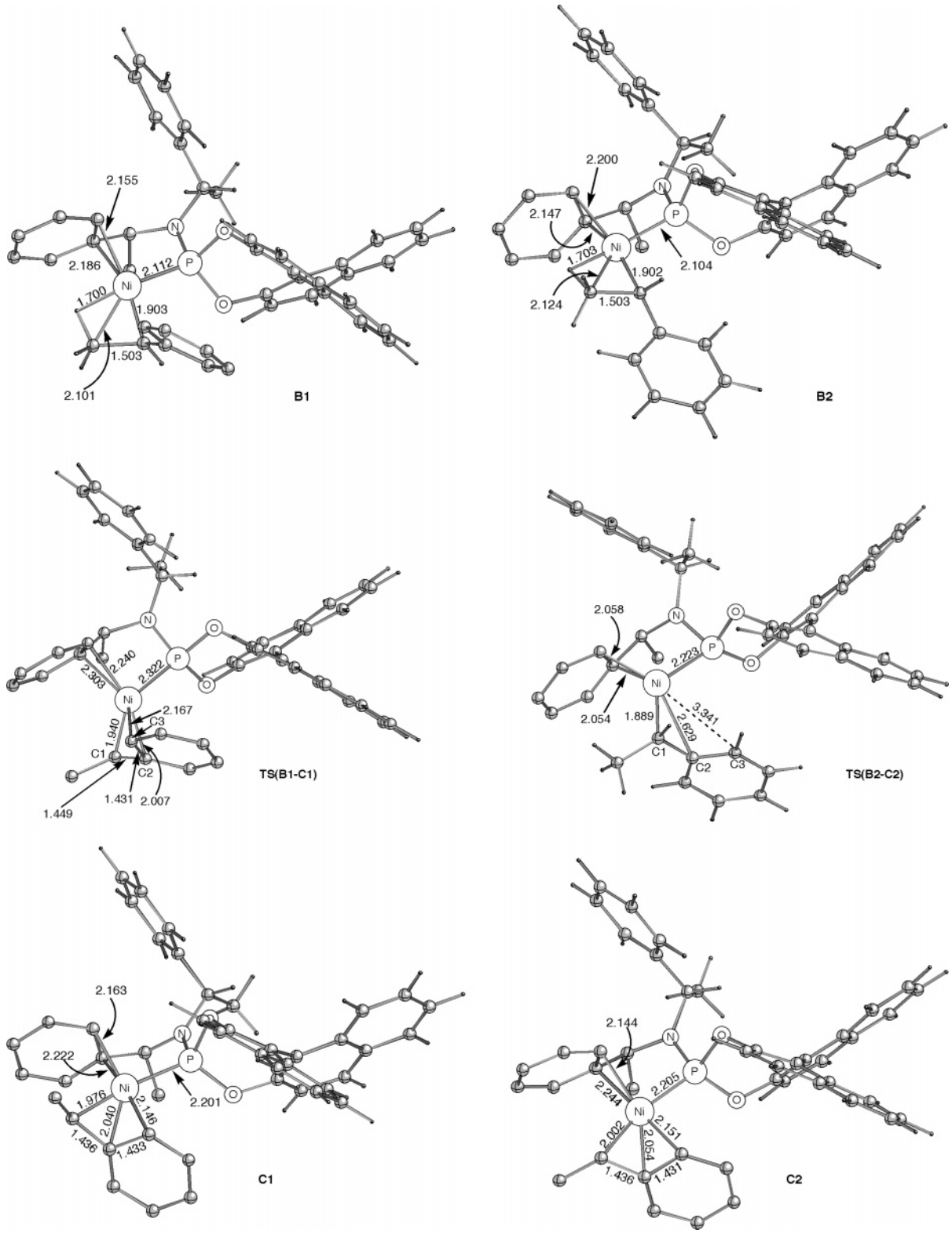

Figure 3. Calculated geometries of **B1**, **B2**, **C1**, **C2**, and transition states **TS(B1−C1)** and **TS(B2−C2)** with selected atom distances [Å] (H atoms were partly removed for clarity).

bound hydride was moved toward the terminal $=CH_2$ group, yielding complexes with Ni−H bond lengths of ca. 1.70 Å (Figure 3, **B3** and **B4** not shown). In these structures the olefinic double bond is elongated to 1.5 Å, indicating its transformation into a C−C single bond, with one of the terminal hydrogen atoms interacting agostically with nickel. In other words, these intermediates are already "on the way" to styrene insertion.

Furthermore we located an isomer of **B1** (**B1a**) in which the styrene molecule is rotated clockwise by 90° and the olefinic double bond coordinates in perpendicular mode (d_{Ni-H}: 1.44 Å; Figure 4). Here the olefinic double bond is expanded from 1.34 Å in free styrene to 1.39 Å, indicating a long, coordinating C−C double bond.

B1 and **B2** are the two most stable diastereomers, with **B1** being slightly more unstable than **B2** by +1.38

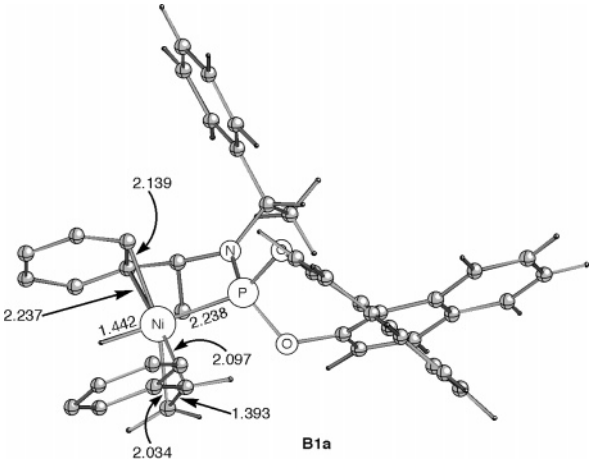

Figure 4. Calculated geometry of **B1a** with selected atom distances [Å] (H atoms were removed partly for clarity).

kcal/mol, meaning that on the computational level chosen **B1** and **B2** have practically the same energy. Concluding from this result they would be expected to exist in the reaction mixture in equal amounts. Diastereomers **B3**, **B4**, **B6**, and **B8** are more unstable than **B2** by +4.02, +4.02, +19.26, and +18.45 kcal/mol, respectively.

Consequently we located the final products of the hydride transfer for **B1** and **B2** as well as the corresponding transition states (Figure 3). The products **C1** and **C2** are more stable than the reactants **B1** and **B2** by −4.89 and −2.32 kcal/mol, respectively. Most striking are the highly different activation energies for this reaction. For the reaction of **B1** to **C1** the transition state **TS(B1−C1)** lies +17.57 kcal/mol above the reactant's energy. However the energy of **TS(B2−C2)** is higher than the reactant's energy by +26.92 kcal/mol and thus indicates an activation energy that is roughly 10 kcal/mol higher than the activation energy of the competing reaction from **B1** to **C1**.

The large difference in activation energies suggests that the reaction should proceed solely via **TS(B1−C1)**. In other words **B3**−**B8** are irrelevant for the reaction, and **B2** reacts so much slower than **B1** that it can be neglected. The sequence starting with **B1** leads to (*S*)-3-phenyl-1-butene as the final reaction product, in full accordance with the absolute stereochemistry observed experimentally. The large difference in activation energies is in line nicely with the high enantioselectivity observed with ligand (R_a,S_C,S_C)-**7**.

An inspection of the transition state structures shows that the nickel center in **TS(B1−C1)** is coordinated by the phoshorous atom, two phenyl ring carbon atoms, and a completely established allyl group (Figure 3). The corresponding Ni−C distances are as follows: Ni−C1 1.940, Ni−C2 2.007, and Ni−C3 2.167 Å. This is different from **TS(B2−C2)**, where the allyl group is not established completely, with carbon atoms C2 and C3 residing too far away: Ni−C1 1.889, Ni−C2 2.619, Ni−C3 3.341 Å (Figure 3). Thus the nickel center in **TS(B2−C2)** has a higher electron demand, which is partly compensated for by a shorter Ni−P distance (2.223 Å) compared to **TS(B1−C1)**, in which the Ni−P distance is 2.322 Å. Also the two coordinating carbon atoms of the ligand's phenyl ring are much closer to the nickel center (2.058, 2.054 Å) than in **TS(B1−C1)** (2.240, 2.302 Å). This compensation is very effective; thus the differences in Wiberg bond indices for nickel as calculated by a NBO analysis[20] are very small (2.34 and 2.33 for **TS(B1−C1)** and **TS(B2−C2)**, respectively).

C−C Bond Formation (C → D). The next step in the catalytic cycle is the coordination of ethylene followed by C−C bond formation. The hemilabile coordination via the phenyl ring in **C1** and **C2** is broken up as ethylene coordinates instead. The resulting compounds **D1** and **D2** are more stable than the reactants by −10.29 and −10.54 kcal/mol, indicating ethylene coordination to be a clearly exothermic process (Figure 5).

In these compounds ethylene is coordinated nearly parallel with respect to the best plane spawned by P−Ni−$C2_{allyl}$ and is thus already in the correct orientation for the subsequent reaction. We also located diastereomers **D1a** and **D2a** with ethylene coordinated perpendicular to the P−Ni−$C2_{allyl}$ plane (not shown). These compounds have by and large the same stability as the ones with parallel ethylene coordination (−0.69 and −2.00 kcal/mol for **D1a** and **D2a**, respectively). However, prior to reaction the coordinated ethylene would have to rotate in these molecules. For **D1** and **D2** we located the corresponding products **E1** and **E2** and found them to be more stable than **D1** and **D2** by −14.11 and −14.18 kcal/mol, respectively, which indicates C−C bond formation to be an exothermic process. As can be deduced from Figure 6 the new carbon−carbon bond is quite long (1.549 and 1.556 Å in **E1** and **E2**, respectively). The geometries of **E1** and **E2** are very interesting. The nickel center forms one Ni−C σ-bond, and interestingly the whole phenyl ring of the former styrene moiety coordinates to the nickel center in η^6-fashion. This is an interesting intermediate possibility for the system to occupy the vacant coordination site at the nickel center intramolecularly without the need to employ other agents (e.g., solvent, counterion). The corresponding transition states **TS(D1−E1)** and **TS(D2−E2)** were located subsequently with activation energies (i) being substantially smaller than for the reaction of **B** to **C** and (ii) showing values with a nonsignificant difference for the reactions of **D1** to **E1** and of **D2** to **E2** (+6.59 and +5.90 kcal/mol, respectively). This suggests that there is no enantiodiscrimination in the C−C bond formation process.

Although from the preceding discussion other diastereomers should not be present at this stage of the reaction, we were curious if an exchange of the positions of ethylene and allyl moiety would result in an alternative reaction pathway. Despite many attempts we were not able to locate **D3** (parallel coordinated ethylene) and only obtained **D3a** (perpendicularly coordinated ethylene). However, both the transition state **TS(D3−E3)** and the product **E3** were located, and relative to **D3a** (perpendicular ethylene orientation) the transition state is higher in energy by +11.67 kcal/mol (also from this reaction path the *S*-enantiomer would evolve as the final

(20) (a) Carpenter, J. E.; Weinhold, F. *J. Mol. Struct. (THEOCHEM)* **1988**, *169*, 41. (b) Carpenter, J. E. Ph.D. Thesis, University of Wisconsin, 1987. (c) Foster, J. P.; Weinhold, F. *J. Am. Chem. Soc.* **1980**, *102*, 7211. (d) Reed, A. E.; Weinhold, F. *J. Chem. Phys.* **1983**, *78*, 4066. (e) Reed, A. E.; Weinhold, F. *J. Chem. Phys.* **1983**, *81*, 1736. (f) Reed, A. E.; Weinstock, R. B.; Weinhold, F. *J. Chem. Phys.* **1985**, *83*, 735. (g) Reed, A. E.; Curtiss, L. A.; Weinhold, F. *Chem. Rev.* **1988**, *88*, 899. (h) Weinhold, F.; Carpenter, J. E. *Plenum* **1988**, 227.

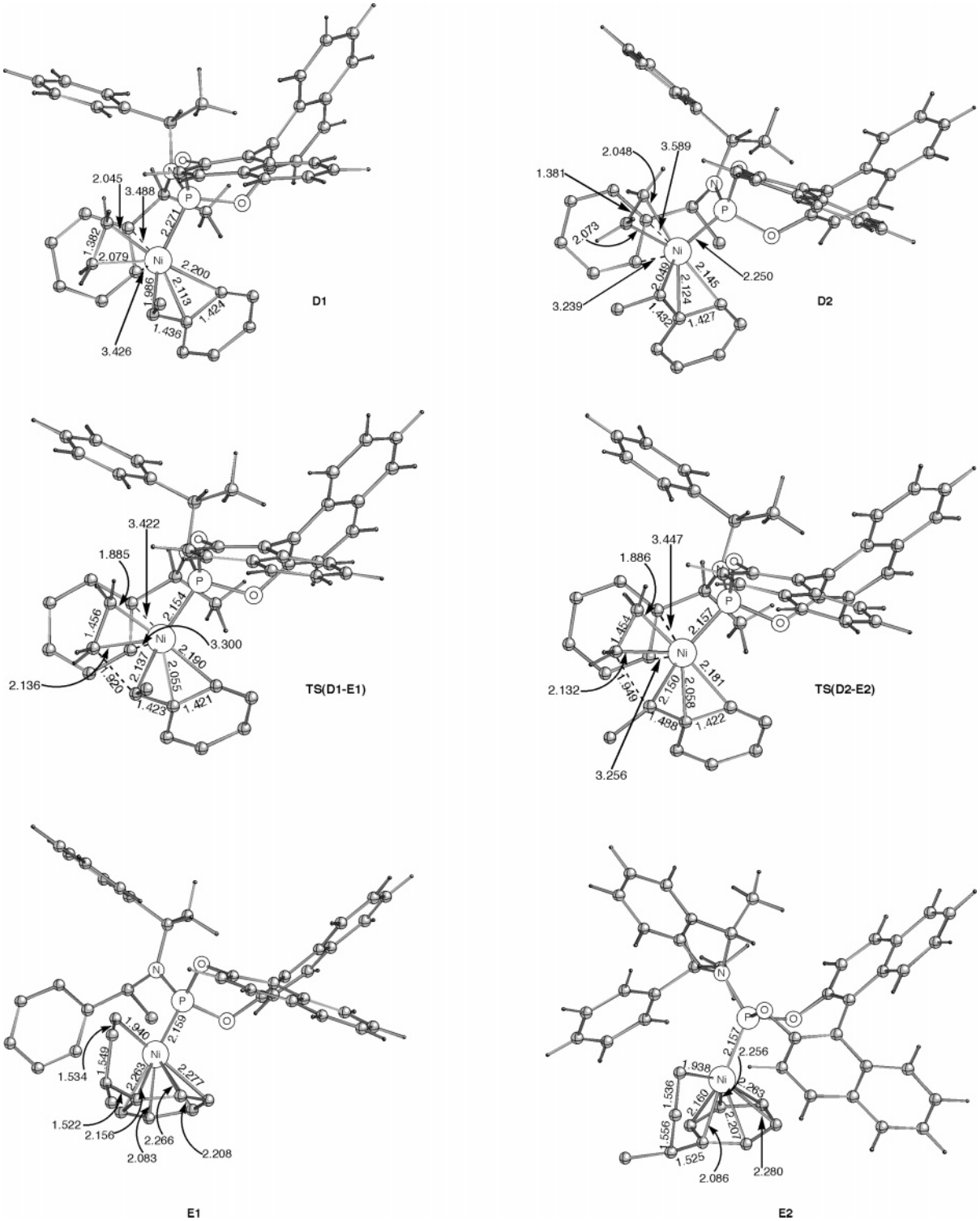

Figure 5. Calculated geometries **D1**, **D2**, **E1**, **E2**, and transition states **TS(D1−E1)** and **TS(D2−E2)** with selected atom distances [Å] (H atoms were partly removed for clarity).

product). As a result, even if the reaction could proceed starting from **D3a**, which is doubtful, the activation energy is much higher than with **D1** and **D2**, and thus this reaction path can be ruled out. The final possibility—which would eventually yield the *R*-configurated product—starts with **D4**. We located both the **D4** (ethylene parallel) and the **D4a** conformer and also the product **E4**, but despite many attempts we failed to obtain the structure of the transition state **TS(D4−E4)**. This is a strong hint that this reaction path does not exist. From these results it follows that the reaction will proceed only via **D1** and **D2**. The complete energy profile obtained is shown in Figure 6.

In the next step of the mechanism the hydrovinylated endproduct would be released via a β-hydrogen elimination, and preliminary calculations on model systems have shown this step to be strongly endothermic, which is in accordance with calculations carried out for similar complexes.[21] This step will be investigated further in the future.

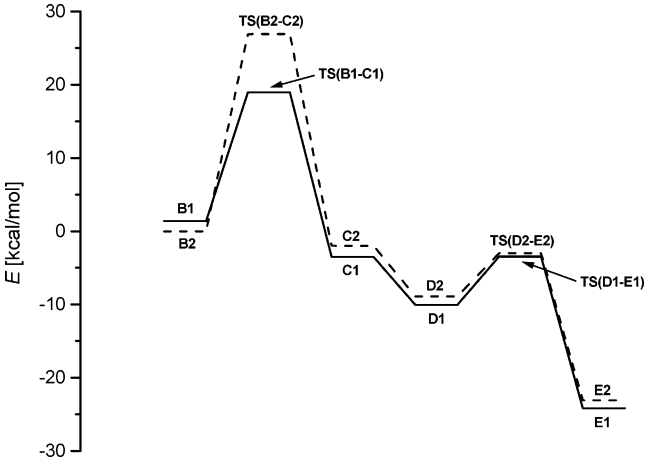

Figure 6. Energy profiles for reactions from **B1** to **E1** (—) and **B2** to **E2** (- - -).

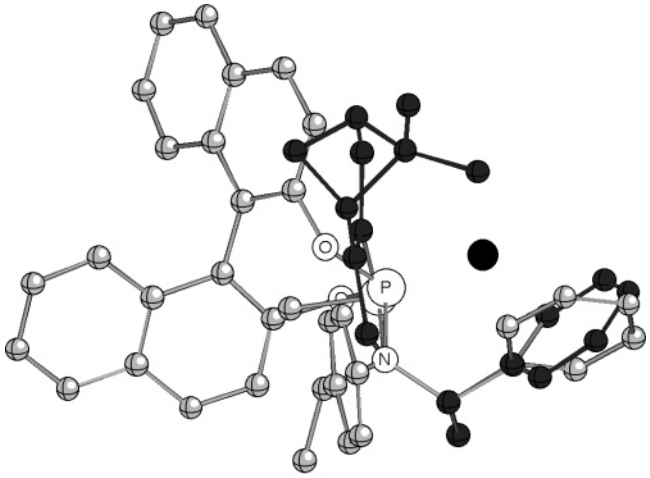

Figure 7. Superimposition of the solid state structures of (R_a,S_c,S_c)-**7** (light gray) and azaphospholene *all-(S)*-**4** (dark gray, only one-half of the ligand is shown; hydrogen atoms were omitted for clarity). For orientation the area in which the nickel center resides in the complexes is marked with a black circle.

Structural Key Features of Ligands 7 and 4. When the chemical functionalities of (R_a,S_c,S_c)-**7** and Wilke's azaphospholene ligand **4** are compared, it is tempting to suspect similar key structural features within the amido substituents of both ligands. Indeed the similarities of the structures are striking: Figure 7 shows a superimposition of the solid state structures of (R_a,S_c,S_c)-**7** and Wilke's azaphospholene **4** (*all*-(*S*)-form), with the P−N−$C_{H(Me)(Ph)}$ bonds of the two ligands superimposed on each other. It is interesting to note that the whole region of (R_a,S_c,S_c)-**7** involved in coordination of the nickel center is structurally so similar compared to *all-(S)*-**4** that it suggests the two ligands operate in essentially the same way. In other words this means that (R_a,S_c,S_c)-**7** mimics Wilke's ligand successfully. This means also that with (R_a,S_c,S_c)-**7** a replacement for azaphospholene **4** was designed, which is much easier to synthesize. Furthermore this result can be used as a basis for rational ligand development for C−C bond forming reactions which are similar to the hydrovinylation and proceed at cationic nickel centers.

Role of the Anion and the Solvent. Our experimental work showed chloride abstraction of the precursor complex [{Ni(allyl)Cl}$_2$] with NaBARF and $NaBF_4$ to result in active and inactive catalyst systems, respectively, whereas activation with $LiNTf_2$ results in a moderate activity. Similar pronounced anion effects were reported by Wilke[3b] and RajanBabu.[8d] To help rationalize these experimental results, we set out to investigate the intrinsic influence of the presence of different anions computationally. Therefore we calculated the structures and energies of type **C** complexes in the presence of BF_4^- and $BARF^-$ ions and without the presence of anion.

Since the calculations without anion as described in the preceding subsections showed that **C1** is most likely the predominant diastereomer prior to ethylene coordination, we chose it for the introduction of anions. We positioned the BF_4^- ion "arbitrarily" at four different points in space (**C1(BF$_4$)-1** to **-4**) and performed geometry optimizations of these systems. The intention was to let BF_4^- approach the complex from every side. For one starting geometry (**C1(BF$_4$)-4**) the BF_4^- ion was directly placed under the nickel center. We note our awareness of the fact that such a screening of possible anion locations is by far not complete. However, we are convinced to obtain a qualitatively correct picture, since the Mulliken charges of **C1** without the presence of anion are distributed very regularly over the whole molecule. All atoms including nickel bear positive or negative charges with very small deviations from zero; the only exception is the phosphorus atom, with a charge of +1.10, but the P atom is hidden deep in the complex and is not accessible for direct electrostatic interaction. Thus, it can be expected that the fluorine atoms of BF_4^- will form bridges with the most electropositive atoms available on the surface of the complex, i.e., with the hydrogen atoms. The exception might be **C1(BF$_4$)-4**, for which a fluorine−nickel bonding interaction would be expected. The structures obtained for **C1(BF$_4$)-1** to **-4** are shown in Figure 8.

All geometries in which BF_4^- is not coordinated to the nickel center (**C1(BF$_4$)-1** to **-3**) show the anion to be only weakly distorted; that is, there are B−F···H−C bridges as was assumed, but no other directed strong attractive interactions (B−F distances range between 1.388 and 1.442 Å; B−F distance in free BF_4^-: 1.418 Å). As expected the complexation energies are fairly pronounced (**C1(BF$_4$)-1**: −59.80, **C1(BF$_4$)-2**: −63.76, **C1(BF$_4$)-3**: −70.90 kcal/mol), but more important the complexation energy for complex **C1(BF$_4$)-4**, which contains BF_4^- bound to the metal, is substantially larger (−87.54 kcal/mol). This is an indication that if the BF_4^- ion is close to the cationic complex, it will be coordinated as in **C1(BF$_4$)-4** most of the time; that is, chances to find it elsewhere appear to be lower. Furthermore, in **C1(BF$_4$)-4** the geometry of the BF_4^- ion is distorted significantly, with the coordinating fluorine atom being located 1.489 Å away from the boron center (B−F distance in free BF_4^-: 1.418 Å), whereas the other fluorine atoms are significantly closer to boron (d_{av}: 1.396 Å). The Ni−F distance amounts to 2.167 Å and thus indicates clearly a bonding interaction. We recal-

(21) (a) Fan, L.; Krzywicki, A.; Somogyvari, A.; Ziegler, T. *Inorg. Chem.* **1994**, *33*, 5287. (b) Senn, H. M.; Blöchl, P. E.; Togni, A. *J. Am. Chem. Soc.* **2000**, *122*, 4098−4107.

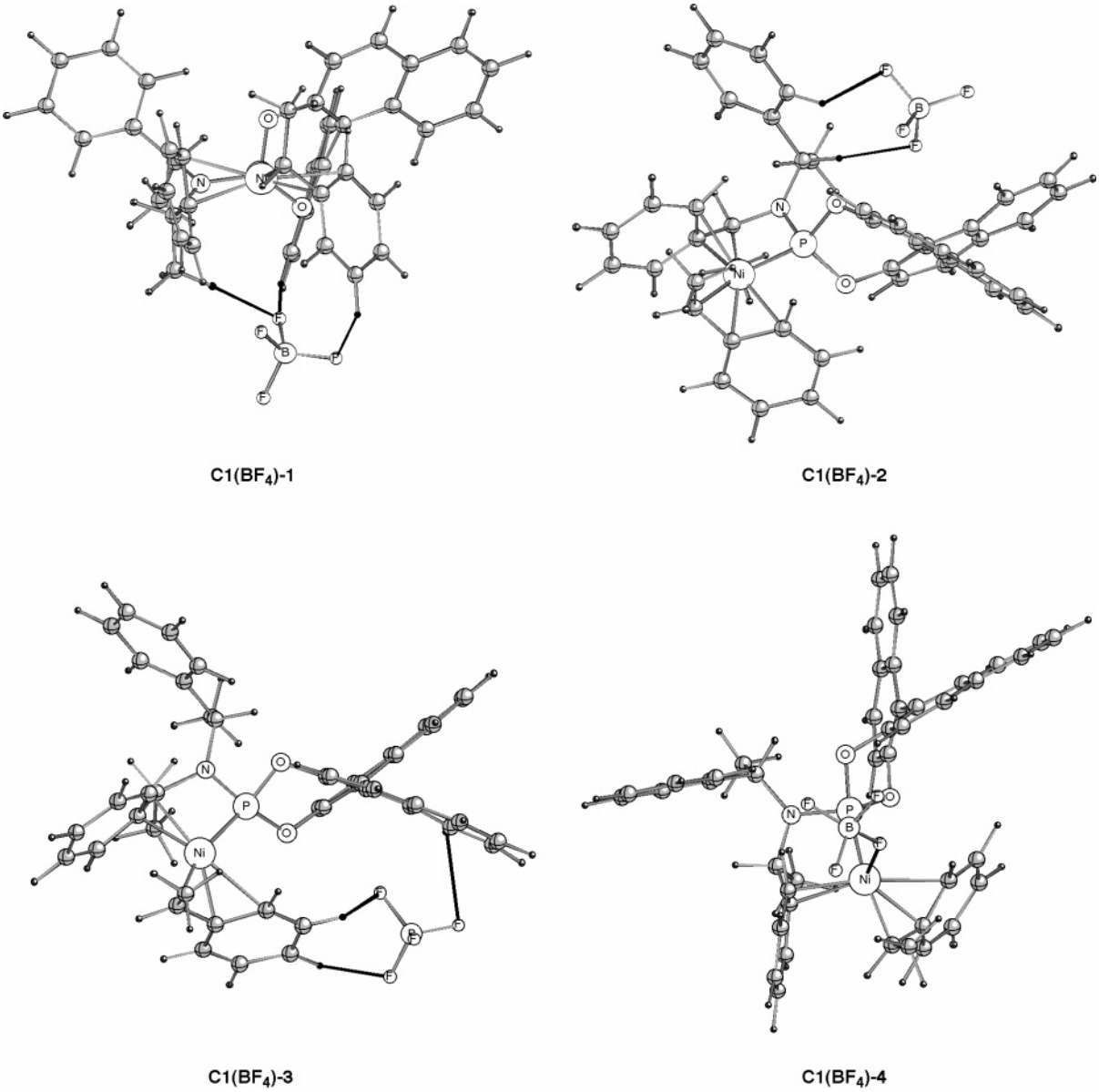

Figure 8. Optimized geometries of the parent complex **C1** together with BF_4^- ion present in different positions. The nickel center is accessible for BF_4^- only in **C1(BF$_4$)-4**. Bold black lines indicate F−H interactions for **C1(BF$_4$)1** to **-3** and F−Ni interactions for **C1(BF$_4$)-4**.

culated the energies of these complexes in the presence of dichloromethane as solvent using the COSMO solvation model[16] and found a stabilization of the complexes, as was expected. The observations outlined above were confirmed: **C1(BF$_4$)-4** is stabilized by −17.76 kcal/mol, whereas **C1(BF$_4$)-1**, **C1(BF$_4$)-2**, and **C1(BF$_4$)-3** are lower in energy than the single cation and anion only by −2.63, −5.40, and −8.22 kcal/mol, respectively. This means, that also in the presence of solvent the position of BF_4^- at the nickel center is clearly favored over the other positions.

In the next step we optimized the geometry of **C2(BF$_4$)-4** (BF_4^- bound to the nickel center, Figure 9), which upon reaction with ethylene yields (*R*)-3-phenyl-1-butene (reaction of **C1(BF$_4$)-4** leads to desired (*S*)-3-phenyl-1-butene) and found **C1(BF$_4$)-4** to be more stable than **C2(BF$_4$)-4** by −3.95 kcal/mol (and −2.32 kcal/mol when the higher level optimizations BP86/TZVP are used; Table 2). This is interesting, since for the anion-free systems the energy difference between **C1** and **C2** is within error range (1.19 kcal/mol; BP86/SV(P)); that is, the anion introduces an energy difference.

Finally we performed calculations employing BARF as the counterion. At first we tried to optimize the structure of **C1(barf)-1**, in which one of the anion's CF_3 groups is as close to the nickel center as was obtained with BF_4^- in **C1(BF$_4$)-4**; that is, we tried to reproduce the Ni−F bonding interaction that was obtained before with BF_4^-. As a result of the calculations, the BARF anion was moved away from the cationic complex, and in **C1(barf)-1** the Ni−F distance amounts to 3.445 Å (the C−F distances of this particular CF_3 group are 1.377 [F interacting with Ni], 1.363, 1.360 Å; mean C−F distances in free $BARF^-$: 1.360 Å; Figure 10).

Again this indicates an attractive interaction; however its strength will be significantly lower. The energy released upon formation of **C1(barf)-1** is −40.85 kcal/mol (compare to −87.54 kcal/mol in the presence of BF_4^-). Again in **C1(barf)-1**—which would react to (*S*)-3-phenyl-1-butene—one of the ligand's phenyl rings

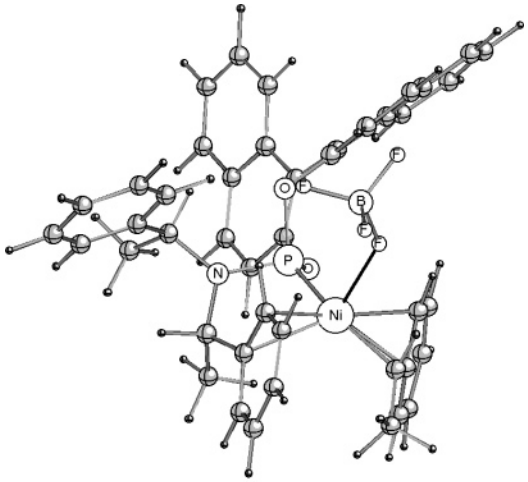

Figure 9. Calculated geometry of **C2(BF$_4$)-4** highlighting the bonding interaction of BF_4^-. The bold black line denotes the F−Ni contact.

completes the coordination sphere around nickel. We also calculated **C2(barf)-1** (reacting to (*R*)-3-phenyl-1-butene) and found it to be practically of the same stability (+2.07 kcal/mol) relative to **C1(barf)-1**. Furthermore we optimized geometries in which the BARF anion is located at other positions around the cation (**C1(barf)-2**, **C1(barf)-3**); however these structures also were slightly less stable than **C1(barf)-1** (stability order [kcal/mol]: **C1(barf)-1** (0.00) < **C1(barf)-2** (+2.70) < **C1(barf)-3** (+3.14)). In these compounds H−F bridges between one fluorine atom of a CF_3 group and a hydrogen atom of the ligand or the styrene moiety are observed. As with BF_4^-, the structures containing BARF were also subject to calculations including solvent effects. Interestingly the calculations using the COSMO solvation model resulted in vanishing energy differences with a formal stability order **C1(barf)-2** < **C1(barf)-3** < **C1(barf)-1** < **C2(barf)-1** (relative energies are 0.00/+0.06/+0.38/+2.32 kcal/mol). Practically this means that these compounds have the same energies; that is, energetically it does not make a difference if there are F−H bridges or a F−Ni bonding interaction. In other words, chances of finding the BARF anion at one of the positions calculated appear to be equal, which is in contrast to the BF_4^--containing systems, where coordination at the metal was clearly preferred.

To shed light on the influence of the counterion for the reaction itself, we chose the C−C bond forming step for calculations using a model ligand as shown in Scheme 4. We tried to localize the same stationary points with BF_4^- present at the metal as discussed before for systems containing the real ligand and no counterion. Interestingly we found the product **E(BF$_4$)** to be as stable as the reactant **D(BF$_4$)** (−1.07 kcal/mol), but more important is the fact that despite several attempts we did not succeed in locating the transition state of this reaction (Scheme 4).

We consider this as a hint at the electroneutral complex to be inactive for the C−C bond formation. In other words, the complex is catalytically active only at times, when the anion is far away enough to render the metal complex cationic. The complete picture emerging from the results of this subsection suggests BARF-containing systems to be more reactive than BF_4^--containing systems of this kind. Actually the calculations suggest that the BF_4^- systems should be catalytically inactive, which is again in full agreement with experimental data. However, we also note that the experimentally observed inactivity with BF_4^--containing systems might also be associated with the chloride abstraction from the precursor complex.

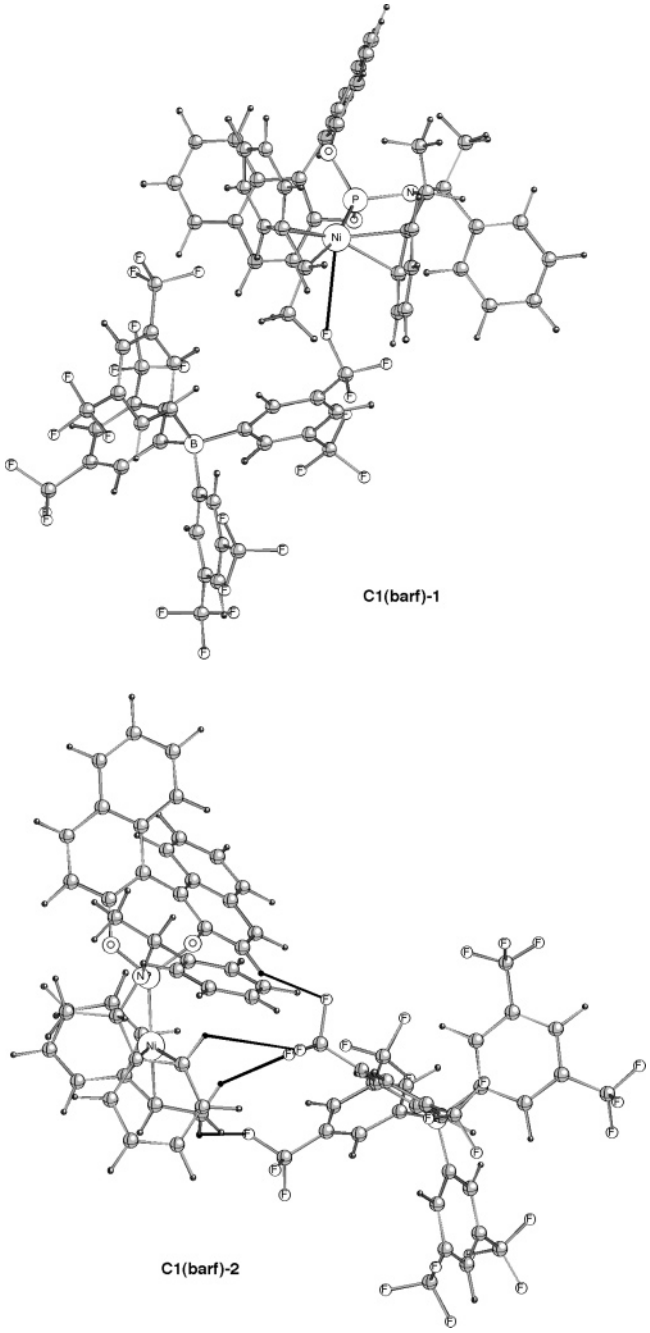

Figure 10. Calculated structure of **C1(barf)-1** (top) and **C1(barf)-2** (bottom) highlighting the interactions with the cationic complex via Ni−F contact and F···H−C bridges, respectively (bold black lines).

Summary

In this work we have examined key steps of the generally accepted reaction mechanism for nickel-catalyzed hydrovinylations using density functional calculations in order to elucidate the influence of phos-

Scheme 4. Stabilitiy of $E_{ML}(BF_4)$ Relative to $D_{ML}(BF_4)$ [kcal/mol][a]

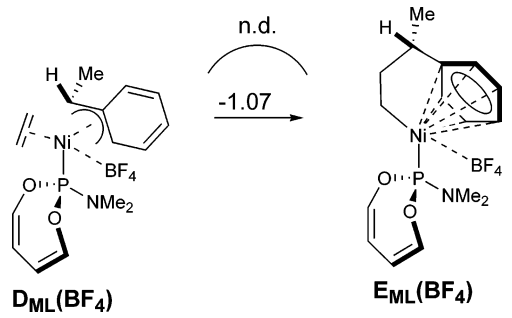

[a] The transition state could not be located (n.d.: not determined, ML = model ligand; see text).

phoramidite (R_a,S_c,S_c)-**7** on the enantioselectivity of the reaction, considering also the role of the anion to a certain extent. The fundamental results are as follows: Of eight theoretically possible diastereomers **B** evolving from the coordination of styrene to the nickel hydride **A**, there are only two diastereomers, **B1** and **B2**, that are chemically plausible, spatially possible, and energetically favorable to start the catalytic cycle. The two diastereomers, which result from coordination of the pro(R) or pro(S) enantioface of styrene show no energy difference, which on the computational level chosen would imply practical consequences; that is, the same amounts of both diastereomers should be present in the reaction mixture. **B1** can react to **C1** by insertion of styrene into the Ni−H bond passing over a transition state with an activation barrier of +17.52 kcal/mol, whereas **B2** needs to pass an activation barrier of +26.92 kcal/mol. This result indicates that **B2** contributes to the reaction negligibly; that is, enantioselectivity is the result of this high difference in activation energies. The pathway originating from **B1** leads ultimatively to the product with *S* configuration, in line with experimental results.

The existence of only two plausible starting structures **B1** and **B2** is the result of the ligand's unique property to help in saturating open valencies at the nickel center by coordinating in a hemilabile way via two carbon atoms of one ligand phenyl group. Eventually during the course of the reaction this coordination must be broken up with ethylene occupying the corresponding coordination site at the metal. The subsequent C−C bond formation (**D** → **E**) has a low lying activation energy and does not determine enantioselectivity since the activation energies of the two reaction paths are the same on the computational level chosen (**TSD1-E1**: +6.59 and **TSD2-E2**: +5.90 kcal/mol).

For complexes **C** the anions BF_4^- and $BARF^-$ can occupy various positions around the cationic complex. There is a very clear (BF_4^-) and moderate ($BARF^-$) preference for positions in which bonding interactions between fluorine atoms of the anion and the nickel center of the cation are possible. For the $BARF^-$ anion this interaction is no longer favored when solvent effects are taken into consideration. A model calculation has shown that bonded BF_4^- ion renders the transition metal complex catalytically inactive. In turn this means that dissociation of the anion is necessary to enable the reaction within the coordination sphere of the nickel center.

In summary, our results demonstrate the importance of hemilabile coordination of phenyl groups in the hydrovinylation mechanism. In fact, there is a striking similarity of the key structural features of ligand (R_a,S_C,S_C)-**7** and Wilke's ligand, which is the only other ligand providing similar activities and selectivities. Further experimental and theoretical work based on these guidelines for ligand design is in progress.

Acknowledgment. This work was supported by the Deutsche Forschungsgemeinschaft (SFB 380). X-ray structure data collection by Arbeitskreis Strukturchemie, Prof. Dr. U. Englert, Inst. of Inorganic Chemistry, RWTH-Aachen, is gratefully acknowledged. We thank Dr. Jan. Runsink, Inst. of Organic Chemistry, RWTH-Aachen, for detailed NMR investigations of (R_a,S_C,S_C)-**7**. Generous allocation of computer time by the Hochschulrechenzentrum (RWTH-Aachen) is gratefully acknowledged.

Supporting Information Available: Crystallographic data of (R_a,S_c,S_c)-**7** (cif file) is available free of charge via the Internet at http://pubs.acs.org.

OM040107L